Single-sensor Motion and Orientation Tracking in a Moving Vehicle

Çağdaş Karataş, Luyang Liu, Marco Gruteser, Richard Howard,
WINLAB, Rutgers University, North Brunswick, NJ, USA
{cagdas, luyang, gruteser, reh}@winlab.rutgers.edu

Abstract—Given the increasing popularity of mobile and wearable devices, this paper explores the potential use of inertial sensors that are widely available on mobile and wearable devices for vehicle and driver tracking. Such a capability would enable novel classes of mobile safety and assisted driving applications without relying on information or sensors in the vehicle. Although inertial sensors have been widely used in motion tracking, existing approaches cannot distinguish the motion of the vehicle and the device's motion in the vehicle. Additionally, the noise exerted from the electronic components in the vehicle and the ferromagnetic frame of the vehicle distorts the inertial sensor readings. This paper introduces a method to separately estimate the orientation of both the vehicle and the sensor by tracking the earth's magnetic field and the electromagnetic distortion from the vehicle, as measured by a magnetometer in addition to a gyroscope and an accelerometer. Specifically, the vehicle noise is used to estimate the orientation of the sensor within the vehicle while the earth's magnetic field combined with vehicle noise is used to estimate the vehicle's heading. Our on-road experiments show that the technique is able to estimate the sensor orientation with a mean error of 5.61^o for the yaw angle and 3.73^o for the pitch angle, as well as able to estimate the vehicle heading with a mean error of 4.12^o.

Index Terms—Orientation Estimation, Driver Activity Tracking, Wearable computing, IMU Sensors, Smartphone-based sensing, Driver Safety

I. Introduction

Inertial sensors on wearable and mobile devices have led to a great number of applications in activity tracking and have created new forms of human-computer interaction. Their use in driving applications can enable new unobtrusive advanced assisted driving systems and safety applications without relying on sensors installed in the vehicle. Providing such services from a single device allows quicker dissemination of new safety services into legacy vehicles and eliminate the problems related to multiple sensors. The sensor placed on the driver's arm as a smartwatch or a fitness tracker could detect driver's arm movements and could be used to estimate steering wheel movements [13], [16] which then could be utilized for many driving safety and assisted driving applications. Additionally, inertial sensors in head-mounted devices such as Google Glass could be used for tracking the driver's head movements as in Fig. 1. Such movements could give accurate information about the driver's focus of attention or lack thereof. Head tracking could be used to enable assisted driving applications by providing contextual information or warnings to drivers based on where the driver turns his head. Such services require
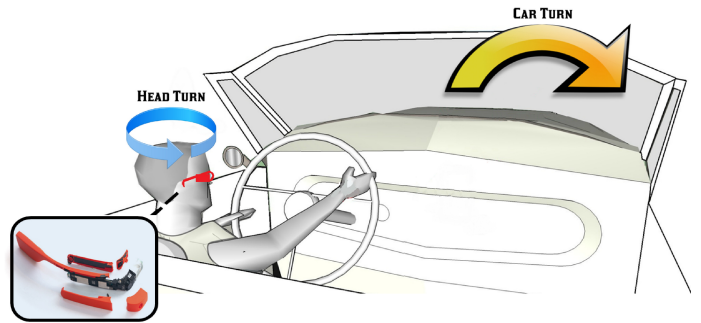
Fig. 1. An example inertial sensor placement on the head mounted device such as Google Glass

accurate tracking of vehicle motion and the mobile's sensor orientation in the vehicle.

Existing solutions. Nowadays, many vehicles come with seat occupancy sensors. Some newer models of vehicles come with driver tracking technologies based on a driver's steering wheel movements [3], [4] or eye tracking [6]. However, these approaches require manufacturers to place sensors in the vehicle and most of these sensors are only available in newer and pricier car models. In order to make this feature more available in other vehicles, researchers have used mobile phones to track driver head movements by using smartphone cameras [24], [1]. Although this approach removes the burden of sensor placement, the driver activity tracking provided by these models are very limited and susceptible to visual occlusions. Additionally, these methods utilize computationally expensive machine vision methods. Only recently have there been studies investigating the use of wearable devices to track driver behaviors [13], [27]. Although these methods estimate both the vehicle's and the user's movements, they require an additional reference sensor to be placed in the vehicle to separate the mobile device's movements from those of the vehicle reference frame.

We propose a single-sensor motion and orientation tracking method that does not require an additional reference sensor to track the vehicle's motion. The method is able to separate the vehicle's motion from the sensor's motion in a moving vehicle even when the motions occur simultaneously. The method estimates the vehicle's magnetic field which occurs naturally due to ferromagnetic materials used in the vehicle and utilizes this magnetic noise as a reference to vehicle's heading direction. The method then uses the relative angles between
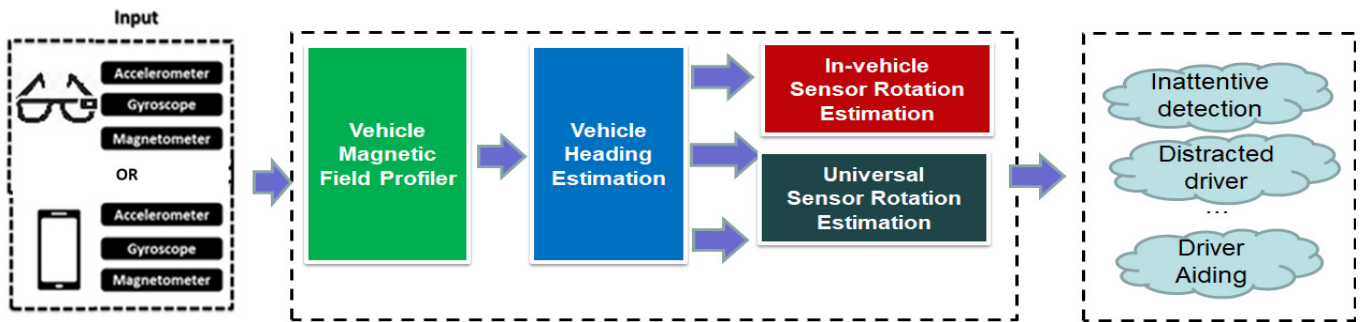
Fig. 2. System overview

vehicle's magnetic noise and earth's magnetic field to estimate the vehicle's heading angle as well as sensor's yaw and pitch angles. We studied how the measured magnetic field changes as the vehicle and the sensor rotate and developed models to estimate the vehicle's heading angle from magnetometer measurements.

The contributions of our work are summarized as follows:

- Analyzing the magnetic noise in the vehicle and modeling how magnetic field measurements change during vehicle and sensor turns.
- Providing a mechanism that can estimate the characteristics of the vehicle's magnetic noise in the vehicle for orientation estimation.
- Proposing an approach that eliminates the reliance on multiple sensors, which previous studies had utilized, and evaluating the method with field experiments.

II. BACKGROUND

There have been active research efforts in reinforcing driving safety by tracking driver's behaviors leveraging mobile sensing technologies on the smartphone (including using cameras, embedded sensors, and other auxiliary devices such as OBD-II in mobile devices or vehicles). In particular, several previous studies use cameras placed on the vehicle to track driver attention and predict driver maneuvers. Oliver et al. [19] use manually annotated driver's gaze from cameras placed in the vehicle to predict driver maneuvers such as lane change and turning. However, this approach needs information about where the driver's visual attention is focused, which is not readily available on current HMD and mobile devices. Several other studies [14], [9] gathered head or eye poses with computer vision techniques and used machine learning algorithms to predict the maneuvers. These studies reveal the correlation between driver's head movements and vehicle's maneuvers. Doshi et al. [9] also state that head pose tracking systems are more robust than gaze tracking and for the lane change detection systems head pose is a better cue than eye gaze.

In contrast, other works rely less on specific phone placement and more on motion sensing through phone's embedded inertial sensors. Chen et al. [8] develop a vehicle steering detection middle-ware to detect various vehicle maneuvers, including lane changes, turns, and driving on curvy roads.

Liu et al. [17] design a simple setup to collect useful driving data for self-driving with a smartphone. Castignani et.al. [7] propose SenseFleet, a driver profile platform that is able to detect risky driving events independently on a mobile device. Wang et al. [27], [28] utilize embedded sensors in a smartphone and a reference point (e.g., an OBD device) in the vehicle to determine whether the phone is on the left or right side of the vehicle. However, most of these approaches can only infer the vehicle's motion based on the inertial sensing measurements from the smartphone, which can hardly track driver behavior inside the car.

The emerging market of wearable devices provides the opportunity to track the motion of human body components. For example, wrist-worn smartwatches or fitness bands can be used to track human's hand and arm [23], [26], [21], [25], while smartglasses and other head-mounted displays (VR, AR) can be used to track head positions and orientations [15], [11], [32], [10]. However, tracking human body inside the vehicle is challenges. As the vehicle is a non-inertial system, the motion of the vehicle generates large noise to the inertial sensor measurements, which significantly reduce the tracking accuracy of those previous algorithms. Previous works [13], [17], [12] use the inertial sensor measurements from both the smartphone and smartwatch to estimate the human motion. The basic idea is to use the smartphone to track vehicle motion, and derive the human motion inside the car by eliminating the vehicle motion from the smartwatch. However, this approach requires both the smartphone and smartwatch to work jointly. In our work, we can track both the vehicle and human motion with only one single inertial sensor, leveraging the in-vehicle magnetic noises. The idea of using the magnetic noise from surroundings for sensing purposes has been adopted in several previous works, including parking space sensing [2], human walking direction sensing [22], and near-field communication [20]. Our work turns the vehicle's magnetic noise from foe to friend, and use it to differentiate the in-vehicle human motion with the vehicle motion.

Applications. Estimating the sensor's and the vehicle's movement from a single-sensor could enable many useful applications and eliminate the problems related to multiple sensors in prior models mentioned above. The sensor placed on the driver's arm as a smartwatch or a fitness tracker could
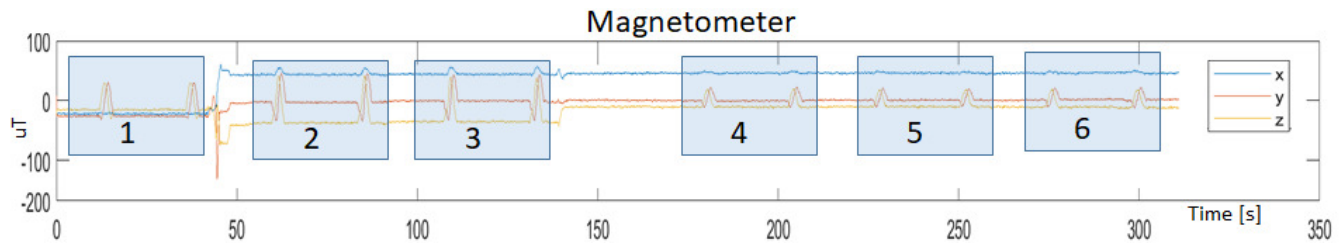
Fig. 3. Magnetic field measurements 1) Outside of the vehicle 2) On Vehicle floor, Engine off 3) On floor, Engine on 4)On seat, engine off 5) On seat, engine on 6) On seat, Vehicle Moves. The small peaks occurs when sensor rotates along its x-axes

detect proper steering such as whether the driver turned the steering wheel properly when making a turn or is able to keep the vehicle in the lane. This model can detect any inconsistency between the steering wheel and the vehicle movements. In turn, this data can be used to detect external factors, such as sliding vehicles due to road conditions. Then, such information can be crowd-sourced to warn other drivers. Drowsy driving can be also detected by comparing inconsistencies in the driver's steering through wearable sensor's such as smartwatches. Similarly, arm tracking models could also enable gesture-based interactions with infotainment systems. For example, the driver may be able to turn the volume up or down with arm movements over the steering wheel without actually turning the steering wheel, creating a safer driving experience with fewer distractions.

Another body of applications could be enabled by inertial sensors in head-mounted devices such as Google Glass. Head-mounted devices could be used for tracking the driver's head movements. Such movements could give accurate information about the driver's focus of attention or lack thereof. Headtracking systems could detect the driver's errors such as not checking the mirrors before changing lanes or not checking the sides for oncoming traffic before making a turn at an intersection. Head tracking data could be used to enable assisted driving applications by providing contextual information or warnings to drivers based on where the driver turns his head. Just like inertial sensors on smart-watches, head-mounted devices can be also used for simple interactions with the infotainment system. A nodding gesture could be detected by the sensor to select or affirm the option on the current infotainment system. All of such applications will create a safer driving experience for the driver and eliminate distractions which may otherwise be caused by such wearable devices.

Compared to previous work, our approach does not rely on the sensors that may not be found in every vehicle. Additionally, the method does not require computationally intensive computer vision algorithms and does not suffer from visual occlusions. The primary advantage of the method is that it only requires single device with inertial sensors that can be found in most of the mobile and wearable devices.
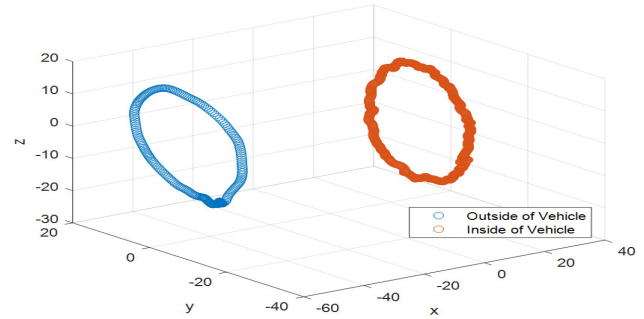
Fig. 4. Magnetometer readings inside and outside of the vehicle when earth's magnetic field rotate

III. System Design

Figure 2 illustrates the system overview of the proposed single-sensor tracking approach. Our method first profiles the characteristics of the vehicle's magnetic field from magnetometer readings. The parameters calculated in the profiling stage can then be used to correct vehicle noise from the inertial sensor readings to estimate the vehicle's heading direction. Finally, sensor's rotation with respect to the vehicle is estimated from vehicle's heading, profile parameters, and sensor readings. Furthermore, Sensor's orientation with respect to the earth can be calculated from the vehicle's and sensor's orientation.

A. Challenges

The main challenges lie in separating the vehicle's motion from the sensor's motion in the vehicle by using a single sensor. The inertial sensor readings are affected by both the vehicle's movements and the sensor's movements. As an example, the accelerometer readings taken from a head mounted device will be affected by the linear acceleration of the head, centripetal force due to the head turn, linear acceleration of the vehicle, the centripetal force due to vehicle turn and gravity. In addition to this ambiguity in the source of the movement, there are many sources of noise that exist in the vehicles such as vibrations and magnetic noise due to the vehicle's ferromagnetic structure. Although the vibrations could be eliminated by using low-pass filters, the magnetic noise constitutes a greater problem that requires further attention. Inertial sensors utilize magnetometers as a 3D compass to track the magnetic north
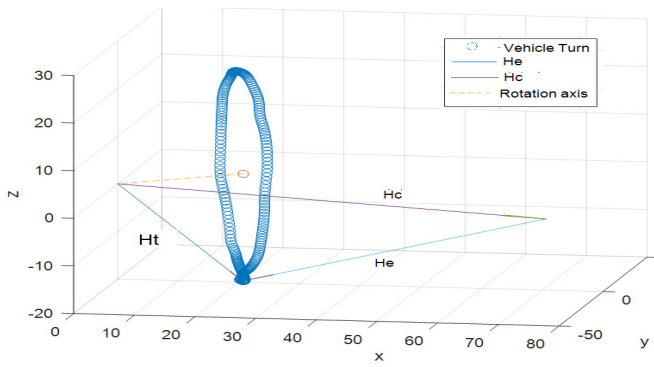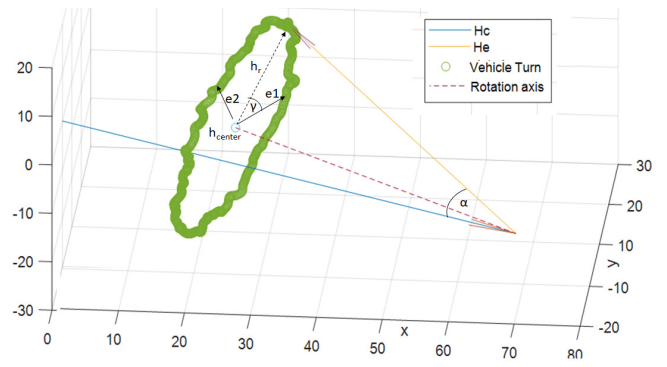
(a) Sensor Turn   (b) Vehicle Turn

Fig. 5. Vehicle's magnetic noise ($\mathbf{H_v}$), Earth's magnetic field ($\mathbf{H_e}$) and Sensor measurement ($\mathbf{H_t}$) during a) sensor turn b) vehicle turn

pole of the earth. This, combined with the gravity measured by the accelerometer, is used to estimate the orientation of the sensor in the North-East-Down (NED) coordinate frame. However, the magnetometer readings exhibit a shift due to the magnetic noise in the vehicle. Furthermore, the magnetic noise depends on the metallic structure of the vehicle as well as the sensor's proximity to the metallic surfaces. Therefore, there is a greater challenge in eliminating the effect of magnetic noise on the sensor's movements and hence, the data collected. Moreover, one could expect that the magnetic noise in the vehicle can also be affected by the means of the changes in the electrical signals in the vehicle. In our experiments, however, we have not observed such a change around the driver/passenger seat area where the users usually use their wearable devices.

B. Approach

The unique insight is to exploit the vehicle's magnetic noise, which is normally considered a problem, as a beacon for vehicle's orientation. By keeping track of vehicle's magnetic noise and the earth's magnetic field, we estimate the vehicle's heading and the sensor's orientation in the vehicle. During vehicle or sensor turns, the magnitude of earth's magnetic field and the vehicle's magnetic noise remain constant. However, the direction of these magnetic fields might change during vehicle and sensor turns. Therefore, the angle (α) between these magnetic vectors and the total magnetic field measurement will change accordingly. Our approach first estimates the angle between these vectors based on the magnetic field measurement. Then, based on the angle, we calculate the vehicle's heading. Finally, we estimate the sensor's orientation in the vehicle.

We will introduce the characteristics of the vehicle's magnetic field in the next subsection. Then we will define how the magnitude of the magnetic field measurement changes during vehicle and the sensor turns. Finally, algorithms will be introduced in detail.

C. Vehicular Magnetic Noise

Due to ferromagnetic materials used and the electrical current running in the electrical system of the vehicle, the vehicle affects the magnetic field inside the vehicle. Although these effects might vary from vehicle to vehicle, they can be grouped into two categories. First, the hard iron distortion which is produced by materials that exhibit a constant magnetic field and is added to earth's magnetic field. In Fig. 3, we have depicted the magnetometer sensor readings at various positions by holding the sensor stable for a while and then making two turns around its x-axis. The turns around x-axes could be seen as 12 small peaks in the figure. The measurements shown in the first region of the graph are taken outside of the vehicle in an open field and therefore, purely depict the earth's magnetic field. As the sensor rotates on its x-axes, the reading on the y and z-axes also vary in a sinusoidal shape. The second region of the graph shows how the sensor reading changes after the sensor is placed on the floor of the vehicle when the engine is not running. As the sensor is placed in the vehicle, the magnetic field introduced by the vehicle is added to earth's magnetic field.

In the third region, the engine starts running. Regions 4-6 are measured while the sensor is placed on the car seat. We can observe small changes in magnetometer readings around t=150s which is due to sensor's positional change from car floor to the seat. In region 4, the engine is not running. In region 5 engine starts running and finally in region 6, the vehicle starts moving. We can observe that the magnetic field does not change between regions 2-3 and 4-6. Therefore, we can conclude that the magnetic field measurements are mostly affected by the sensor's position in the vehicle and are not affected by the engine run. We believe the static magnetic noise sources are more dominant than the dynamic noise produced by the alternating electrical signals in the vehicle. We have verified this conclusion with three different vehicles, namely Hyundai Tucson, Mercedes Benz GLC, and Honda Civic.

The second body of effects is the soft-iron effect. Soft-iron affects change the magnitude of the magnetometer mea-

surements. In magnetometer readings, soft-iron effects could be observed as different amplitudes on different axes as the sensor rotates in a constant magnetic field such as the earth's magnetic field. In Figure 4, we have plotted magnetic field measurements when the earth's magnetic field rotates in the case of the sensor is outside of the vehicle (blue circle) and inside of the vehicle (red circle). To obtain the data points in the blue circle, we have simply rotated the sensor outside of the vehicle and measured the earth's magnetic field. For the sensor, this will result in the earth's magnetic field rotating around it. However, rotating the sensor does not result in depicting only the earth's magnetic field inside of the vehicle since the vehicle's magnetic field is also involved in this test. However, when the vehicle turns, the vehicle's magnetic field is constant and only the earth's magnetic field will be rotating for the sensor. In our experiments, we have not observed significant soft-iron effects inside the vehicle. Therefore, vehicle ignited soft-iron effects has been disregarded for the sake of simplicity.

In addition to hard-iron and soft-iron effects introduced by the vehicle, the electrical components on the sensor board also introduce hard-iron and soft-iron effects. Since any magnetometer sensor zero flux offset is also independent of sensor orientation, it simply adds to the sensor board's hard-iron component and is calibrated and removed at the same time. However, both hard-iron and soft-iron effects are not vehicle specific and require a very standard procedure to calibrate. Therefore, these calibrations are carried out separately and will not be discussed in this paper.

D. Magnetic Field During a Turn

For the purpose of clarity, we introduce how the magnetic field measurements vary as the vehicle or the sensor in the vehicle rotates. As we have explained in the previous subsection, we have neglected the soft-iron effects that vehicle introduces, therefore the vehicle's magnetic field can be simply represented as a vector $\mathbf{h_v(t)}$. Similarly, the earth's magnetic field is denoted as $\mathbf{h_e(t)}$ and sensor measurement $\mathbf{h_t(t)}$ can be calculated as :

$$\mathbf{h_t(t) = h_v(t) + h_e(t)} \tag{1}$$

Additionally from cosine law in vector addition,

$$\|\mathbf{h_t(t)}\|^2 = \|\mathbf{h_v(t)}\|^2 + \|\mathbf{h_e(t)}\|^2 + 2*\|\mathbf{h_v(t)}\| \cdot \|\mathbf{h_e(t)}\| \cdot cos(\alpha) \tag{2}$$

Since, the magnitude of $\mathbf{h_e(t)}$ and $\mathbf{h_v(t)}$ don't change with time, $\|\mathbf{h_t(t)}\|^2$ can be used to calculate α. We will now describe how α changes during sensor and vehicle turn.

Sensor turn in the vehicle. During a sensor turn in the sensor coordinate frame, both the vehicle's magnetic field and earth's magnetic field will be rotating along the rotation axis. Therefore, the sensor will be measured $\mathbf{h_t(t)}$ as a vector rotating along the rotation axis where an example is illustrated in Figure 5a. The measurements will lie on the circle at the base of a cone where the cone's apex is the origin and the slant of the cone is the rotation axis. As the sensor turns, $\mathbf{h_v(t)}$ and $\mathbf{h_e(t)}$ will be constant with respect to each other and the α

angle between them does not change. Hence, the magnitude of the $\mathbf{h_t(t)}$ does not change as well.

Vehicle turn. During the vehicle's turn, the vehicle and sensor turn simultaneously. Therefore, the sensor measures $\mathbf{h_v(t)}$ as a constant. On the other hand, the earth's magnetic field will be rotating with respect to the sensor. This will result in $\mathbf{h_t}$ a circle. The circle would be formed by static $\mathbf{h_e(t)}$ and a rotating $\mathbf{h_e(t)}$ added to $\mathbf{h_e(t)}$. This could be visualized as a cone where the cone's apex is $\mathbf{h_v(t)}$ since it is static and the base circle is formed by rotating $\mathbf{h_e(t)}$ around the apex of the cone. The slant of the cone is the vehicle's rotation axes and γ, vehicle's heading angle is also illustrated in Figure 5b. From Eq.2, $\|\mathbf{h_t(t)}\|$ changes as the vehicle rotates.

E. Initial Vehicle Magnetic Field Profiling

For accurate vehicle heading and sensor orientation estimation, several parameters need to be profiled. The first obvious parameter is the magnitude of the car's magnetic field. The second group of parameters defines how the α angle maps to the vehicle's heading angle. For profiling, we use a single 360° vehicle turn. Although some previous studies [31] require a vehicle turn to sense vehicle dynamics, our approach requires this turn only once for profiling and the same profiling can be used for consecutive trips.

One can assume that $\mathbf{h_v(t)}$ can be simply estimated by subtracting $\mathbf{h_e(t)}$ from $\mathbf{h_t(t)}$. Although $\|\mathbf{h_e(t)}\|$ can be estimated or retrieved from online magnetic field calculators for given latitude and longitude, estimating its direction in the vehicle is not a trivial task. In early stages of our system design, we have tried the following approach: First, measure the earth's magnetic field $\mathbf{h_e(t0)}$ when the sensor is outside of the vehicle right before the sensor enters the vehicle. Then use gyroscope based orientation estimation for a short-time to estimate $\mathbf{h_e(ti)}$. The main reason we relied on gyroscope based orientation is that the magnetometer-based approaches do not work when the sensor enters the vehicle due to vehicle's magnetic field. We have empirically observed that this approach suffers from gyroscope drift problems even when used for a short time period. However, we use $\mathbf{h_{vrough}}$ as a rough estimation to choose one of the two possible candidate points which we introduce in the next paragraph.

As an alternative, we used the $\mathbf{h_t(t)}$ measurements during a 360° vehicle turn. As mentioned in the previous subsection, during the vehicle's turn $\mathbf{h_v(t)}$ should be on the apex of the cone. Therefore by finding the apex of the cone, we can estimate the $\mathbf{h_v(t)}$. Additionally, $\mathbf{h_t(t)}$ measurements lie on the base circle and are $\|\mathbf{h_e(t)}\|$ away from the apex, $\mathbf{h_v(t)}$. For given $\mathbf{h_t(t)}$ measurements during vehicle turn and $\|\mathbf{h_e(t)}\|$, two possible cones could be formed. We choose the cone whose apex is closer to $\mathbf{h_{vrough}}$ and use its apex as $\mathbf{h_v}$ since the gyroscope based estimation and the magnetometer-based estimation must be consistent. Here, $\mathbf{h_v}$ is car's magnetic field for the static reference frame defined by the sensor's coordinate frame during profiling. We choose this coordinate frame as vehicle's coordinate frame and define the heading of the vehicle with respect to this orientation and denote vectors
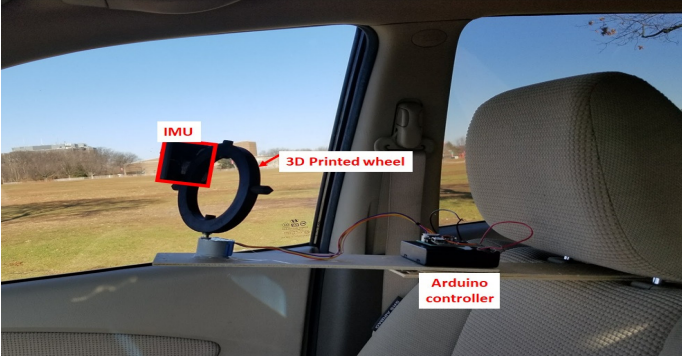
Fig. 6. Arduino controlled sensor setup

Fig. 7. Mean Vehicle Heading Estimation Error when vehicle is placed at 90 to 360 degrees with 90 degree increments. Blue bars indicate mean error, red bars show minimum and maximum error.

represented in this coordinate frame with left superscript such as $^*\mathbf{h_v}$.

In addition to $\mathbf{h_v}$, we define $\mathbf{h_{center}}$ as the center of the base circle. and two perpendicular vectors $\mathbf{e1}$ and $\mathbf{e2}$ as shown in Figure 5b. Although the center of the base circle, $\mathbf{e1}$ and $\mathbf{e2}$ vectors will change with the sensor's orientation in the vehicle, their relationship, such as dot product, with $\mathbf{h_v}(t)$ are independent of sensor orientation and will not change as the sensor rotates.

F. Orientation Estimation

Next, we are going to define equations that we use to estimate the vehicle's heading, sensor's orientation with respect to the vehicle and earth.

Vehicle heading estimation. In order to estimate sensor's orientation, we first need to estimate the vehicle's heading. This requires mapping the angle between $\mathbf{h_e}$ and $\mathbf{h_v}$, α, that we obtained from Eq.2 to vehicle's heading angle γ. First, from dot product rule :

$$^*\mathbf{h_e} \cdot {}^*\mathbf{h_v} = \|\mathbf{h_e}\|\|\mathbf{h_e}\|cos(\alpha) \qquad (3)$$

$^*h_e$ can be also written,

$$^*\mathbf{h_e} = {}^*\mathbf{h_t} - {}^*\mathbf{h_v} \qquad (4)$$

Similarly $^*\mathbf{h_t}$ can be represented as,

$$^*\mathbf{h_t} = {}^*\mathbf{h_{center}} + \mathbf{e_1} * cos(\gamma) + \mathbf{e_2} * sin(\gamma) \qquad (5)$$

where $\mathbf{e_1}$ and $\mathbf{e_2}$ are defined in profiling stage and illustrated in Fig.5b. By combining Eq.3 and Eq.5 and carrying out equations:

$$\gamma_{1,2}(t) = \pm(asin(\frac{\|\mathbf{h_v}\|\|\mathbf{h_e}\|cos(\alpha) - (^*\mathbf{h_{cente}} \cdot {}^*\mathbf{h_v}) + \|\mathbf{h_v}\|^2}{d}$$
$$- asin(\frac{\mathbf{e_2} \cdot {}^*\mathbf{h_v}}{d}))$$

where d is equal to $\sqrt{(\mathbf{e_1} \cdot {}^*\mathbf{h_v})^2 + (\mathbf{e_2} \cdot {}^*\mathbf{h_v})^2}$. Since $asin$ is defined in $[0\ \pi]$, There are two possible γ values. To choose the correct $\gamma(t)$ value, we utilize gyroscope measurements. The algorithm makes an estimate from previous $\gamma(t-1)$ and gyroscope measurement $\phi_x(t)$:

$$\gamma_{estimate} = \gamma(t-1) + \phi_x(t) * \Delta t \qquad (6)$$

and assigns the closest $\gamma_{1,2}(t)$ to $\gamma_{estimate}$ as $\gamma(t)$. However, this selection operation might cause fluctuations in heading estimation. For this reason, we have implemented a temporal filtering approach which requires at least two consequent samples to switch from one selection to the other. This selection process can be improved by better temporal filtering approaches.

In-vehicle Sensor Orientation Estimation. Sensor orientation estimation is straight forward. From given $\gamma(t)$, $\mathbf{e_1}$, $\mathbf{e_2}$ and $^*\mathbf{h_{center}}$, $^*\mathbf{h_t}(t)$ can be calculated from Eq.5. Rotation vector that, $\mathbf{R_{in}}(t)$, transforms $^*\mathbf{h_t}(t)$ to sensor's coordinate frame representation $\mathbf{h_t}(t)$ can be calculated in angle-axes form by using Matlab's built-in command *vrrotvec* with $\mathbf{h_t}(t)$ and $^*\mathbf{h_t}(t)$. Rotation vector than can be converted to rotation matrix, $\mathbf{R_{in}}(t)$, with *vrrotvec2mat* or to euler angles with *rotm2eul* command.

Universal Sensor Orientation Estimation. Sensor's orientation with respect to earth can be calculated by :

$$\mathbf{R_e}(t) = \mathbf{R_{in}}(t) * \begin{bmatrix} 1 & 0 & 0 \\ 0 & cos(\gamma(t)) & -sin(\gamma(t)) \\ 0 & sin(\gamma(t)) & cos(\gamma(t)) \end{bmatrix}$$

IV. PERFORMANCE EVALUATION

During our study, we have conducted two sets of experiments. The objective in the first set of experiments was to estimate the vehicle's heading angle. The second part of the evaluation aims to find the sensor's orientation, namely yaw and pitch angles, by eliminating vehicle's motion from sensor motion. Finally, we compare these results with computer vision based methods and [13] which requires two sensors to estimate the sensor's roll angle.

A. Experiment Setup

We have developed an Arduino controlled setup to simulate sensor movements in the vehicle. The Arduino controller is used to send commands to step motors to turn the sensor to

(a) Sensor Yaw Error

(b) Sensor Pitch Error
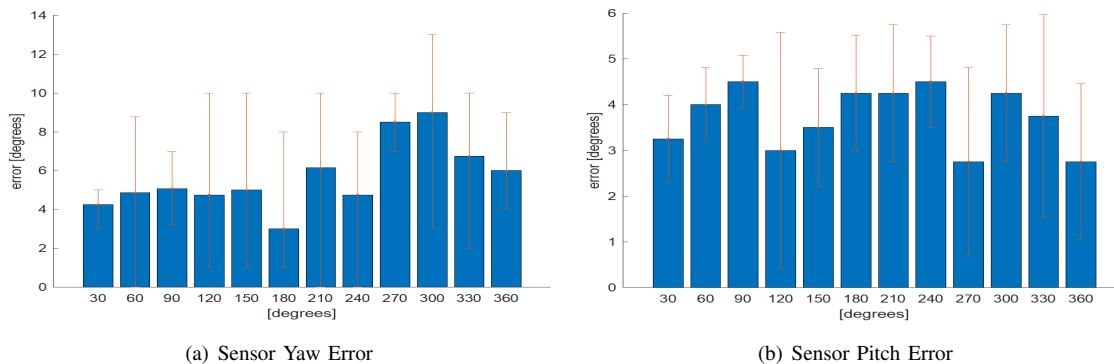
Fig. 8. Mean sensor orientation estimation error when sensor is placed at 30 to 360 degrees with 30 degree increments. Estimation Error for a)Sensor Yaw Angle b) Sensor Pitch Angle. Blue bars indicate mean error, red bars show minimum and maximum error

specific angles. We have placed the sensor on a 3D-printed spinning wheel with one degree of freedom, i.e yaw. Both spinning wheel and Arduino controller are placed on a wooden plank so as to prevent introducing further magnetic noise. The sensor setup is placed in the passenger seat around the headrest position. However, as the sensor rotates, it is possible for the 3D printed wheel to get very close to the headrest, which might have ferromagnetic materials inside. When the sensor approaches any ferromagnetic materials, the magnetic field might vary as the sensor rotates. Therefore, we have empirically chosen a placement point where the sensor is not affected by the ferromagnetic properties of the headrest as it rotates. The sensor placement in the vehicle is shown in Figure 6.

In a standard data collection session, we begin with rotating the sensor 360° placed outside of the vehicle in an open field. We use this data for standard magnetometer calibration. Next, we take the sensor into the vehicle and place it in the aforementioned position. Then we make a 360° vehicle turn while the sensor is fixed for the profiling. The rest of the experiment involves evaluating vehicle heading estimation and sensor orientation estimation with respect to the vehicle. For the vehicle heading estimation stage, we have placed the vehicle at heading angles between 0° to 360° with 90° increments. The heading angles for the ground truth are determined by aligning vehicle with lines at the parking lot which are perpendicular to each other. For sensor orientation estimation, the sensor makes 30° turns between 0° to 360° angles while the vehicle is driven freely without any restrictions such as route, speed, or direction. We placed the step motor vertically and horizontally for yaw and pitch estimation, respectively. We took the input of the step motor as ground truth for sensor orientation estimation. The step motor can be rotated with 2.81^o increments. The experiments are performed by three different drivers and two different cars, a Hyundai Tucson and a Mercedes Benz GLC.

B. Vehicle Heading Estimation Evaluation

In our first experiment, we have tested vehicle heading estimates of the algorithm by rotating the vehicle in 0° to 360° range with 90° increments. The ground truth angles are obtained by aligning the vehicle with the perpendicular

lines in the parking lot. Data is collected at each angle 10 times at different random positions. The results are plotted in Figure 7. The average error is 4.57^o with a standard deviation of 2.97^o. We observed minimum errors when the vehicle is placed at 180°. The error goes as low as 0° degrees for 180° and 360° while goes as high as 10° when the vehicle is placed at 90°. We have observed a mean error of 6.86^o, 3.9^o, 4.61^o, 2.92^o when the vehicle's heading angle is 90°, 180°, 270°, 360°, respectively. We believe the deviations in these errors could be due to vehicle's imperfect placement each time the specific angle is tested since a slight shift in the vehicle parking direction could cause a couple of degrees of error.

The other body of evaluation is conducted when the sensor turns while the vehicle is fixed. The vehicle heading estimate of the system was also fixed as expected with only a couple of exceptions for the data collected sensor orientation estimation. We believe these exceptions occur due to switches in selection from $\gamma_{1,2}(t)$ as mentioned in Section III-F

C. Sensor Orientation Estimation Evaluation

To evaluate the sensor orientation estimation, the sensor is rotated with 30° counter-clockwise increments while the drivers were instructed to drive freely. The results from 480 turns are plotted in Figure 8. We have obtained yaw and pitch angles by placing the Arduino controller setup horizontally and vertically. The results for yaw angle estimation is plotted in Fig. 8(a). We have observed a mean error of 5.61^o with a standard deviation of 3.46^o. We observed the minimum error when the sensor is at 180° and the maximum error when the sensor is at 270°. We also tested the sensor orientation estimation when the sensor is fixed and the vehicle is making 360° turns and observed 8.89^o ripples on average. We believe this residual effect of vehicle turns might be the main source of errors in the yaw estimation.

The results for pitch angle estimation is plotted in Fig. 8 (b). We have observed mean error of 3.73^o with a standard deviation of 1.51^o. Overall, the error was less than 8° and was less than the error we encountered for the yaw angle estimation. This might be due to residual effects of the vehicle turn might be stronger for the yaw angle since both vehicle turns and sensor's yaw rotation are in the same direction. We believe these results could enable many safety applications.

	Mean Absolute Error	
Publication	Yaw	Pitch
Yan[30]	6.72	8.87
Ba[5]	8.8	9.4
Murphy-Chutorian[18]	6.4	5.58
Xiao[29]	3.8	3.2
Single-Sensor	5.61	3.73

TABLE I

THE COMPARISON IN TERMS OF ACCURACY WITH COMPUTER VISION BASED HEAD POSE ESTIMATION STUDIES.

Fig. 9. Comparison of mean error between two-sensor based roll estimation and single sensor based yaw and pitch estimation.

For example, a wrist-worn-sensor based steering wheel tracking system with a standard deviation of 3.90^o could detect vehicle slips greater than 10° with an error rate of 10%. The details of estimation can be found in our previous paper [13].

A comparison of our results with computer vision based head pose estimation methods are given in Table IV-C. We have chosen these studies over many others since they have achieved best accuracy results for different datasets. Yan and his colleagues [30] were able to perform 6.72^o and 8.87^o man absolute error for yaw and pitch estimation on the CHIL-CLEAR07 dataset. Ba and Obodbez [5] proposed a method to estimate head pose with 8.8^o and 9.4^o yaw and pitch errors on IDIAP Head Pose dataset. Murphy-chutorian and Trivedi's head pose estimation system for driver assistance systems was able to achieve 6.4^o yaw and 5.58^o pitch errors on the CVRR-363 dataset. Our single-sensor orientation estimation system was able to achieve higher accuracy than these aforementioned systems without relying on computationally expensive computer vision techniques. On the other hand, Xiao et al [29] recorded a better performance than our approach with 3.8^o and 3.2^o yaw and pitch angle errors on BU Face Tracking dataset. However, this method was only tested for only controlled room environment and the in-vehicle performance is unknown.

Finally, we compared our single-sensor approach to our previous two-sensor approach [13]. In this work, we used the inertial sensors on the mobile phone to track vehicle movements and sensors on a smartwatch to track driver's arm movements. We estimated only arm's roll angle by using fused orientation information obtained from Android API and performance of this approach for yaw and pitch error estimation was not calculated. The comparison is illustrated in Fig. 9. Since this work only was evaluated for $[0^o, 30^o]$, $(30^o, 60^o]$, $(60^o, 90^o]$ roll angle intervals, we are able to compare our system with the results at these angles only. Overall, our system's pitch angle estimation is almost as good as the two-sensor based approach. A 3.4^o mean error was obtained in two-sensor solution while a 3.73^o degree error was achieved in our system. On the other hand, the single-sensor yaw angle estimation with an overall mean error of 5.61^o is less accurate than two-sensor roll estimation. The yaw angle estimation we achieved in our study were 4.25^o, 4.87^o, and 5.07^o while pitch angle estimation accuracy was 3.25^o 4° 4.50^o and two-sensor roll angle estimations of 1.7^o 2.73^o 4.38^o mean errors for sensor angles in $[0^o, 30^o]$, $[30^o, 60^o]$, $(60^o, 90^o]$ ranges was achieved. Overall, the single-sensor algorithm produces slightly less accurate results when compared to the two-sensor studies. These slight differences may be due in part to the
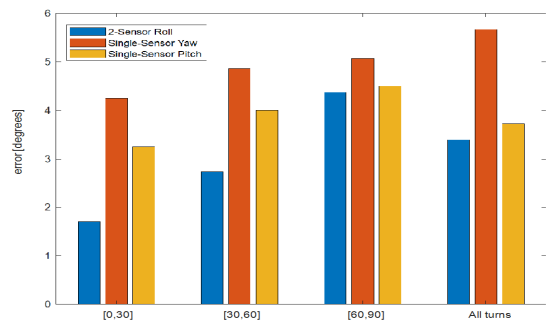
inefficiency of eliminating vehicle movements. Additionally, the two-sensor approach utilizes gyroscope, accelerometer and magnetometer sensors for rotation estimation. In Android API implementation, the orientation is estimated by integrating angular velocity measured through gyroscope and corrected by using magnetometer and accelerometer sensors to eliminate gyroscope's drift error. The pitch and roll angle correction is mostly affected by accelerometer readings since they are perpendicular to gravity. On the other hand, yaw rotation axis is parallel to gravity and gravity measurement doesn't change with the yaw angle. Therefore magnetometer readings are mostly used to correct yaw estimation and more affected by the disturbances and noises in magnetometer data. This might cause larger errors in yaw angle estimation and very similar accuracy results on single-sensor based pitch angle estimation and two-sensor based roll angle estimation. Finally, the methods introduced in this paper

V. LIMITATIONS AND FUTURE WORK

There are several limitations of this work due to the nature of the car's magnetic field. First and most obvious one, similar to a compass at the north/south poles struggling to show the compass heading, the algorithm's accuracy at rotation accuracy would decrease as the earth's magnetic field and gravity vectors have similar directions. In other words, as the earth's magnetic field gets closer to gravity, the information it relays loses its significance. This has another implication for the magnetometer in the vehicle, as the vehicle's magnetic field's direction gets closer to the gravity's direction, it becomes impossible to find the sensor's orientation with respect to the vehicle.

One of the important limitations of this work is that the method assumes the magnitude of vehicle's magnetic field doesn't change. However, the magnetic field might vary as the sensor approaches ferromagnetic materials in the vehicle. We believe the approach will perform especially well where the sensor's translational motion is limited, e.g. head-mounted devices. Also, our system does not use noise cancellation methods such as drift correction. It would be interesting future work to experiment how the performance would be changed by incorporating these methods. The system performance could be improved for changing vehicle magnetic fields in future work. Additionally, analysis of the vehicle's magnetic field

for translational movement might lead to interesting research finding and might be used for sensor positioning.

VI. CONCLUSION

In this paper, we proposed a system that allows monitoring vehicle and driver motion, namely vehicle's heading and sensor's yaw and pitch angles, using only one tri-axial inertial sensor, which may be found in various mobile and wearable devices. It estimates the magnetic noise of the vehicle and its effect on the data through magnitude-based noise estimation method. The approach proposed here eliminates the reliance on multiple sensors, which previous studies had utilized. Reliance on a single sensor, which is directly placed on the body or close vicinity of the driver, can estimate sensor orientation with a mean error of 5.61^o for yaw angle and 3.73^o for pitch angle for our limited dataset while the vehicle was driven freely. We believe this method is especially suitable for head tracking applications where the sensor's translational motion is limited. The data derived from this method can, in turn, be used to determine unsafe driving and help improve driving.

REFERENCES

[1] ionroad. https://ionroad.com/.
[2] Maryam Arab and Tamer Nadeem. Magnopark-locating on-street parking spaces using magnetometer-based pedestrians' smartphones. In *Sensing, Communication, and Networking (SECON), 2017 14th Annual IEEE International Conference on*, pages 1–9. IEEE, 2017.
[3] Mercedes-Benz Attention Assist. https://www.mbusa.com/mercedes/benz/safety#module-3.
[4] Volvo Driver Alert Control. https://www.volvocars.com/us/about/our-innovations/intellisafe.
[5] S Ba and Jean-Marc Odobez. From camera head pose to 3d global roomhead pose using multiple camera views. In *Proc. Int. Workshop Classification Events Activities Relationships*, 2007.
[6] Cadillac Driver Attention Camera. http://www.cadillac.com/world-of-cadillac/innovation/super-cruise.html.
[7] German Castignani, Raphaël Frank, and Thomas Engel. Driver behavior profiling using smartphones. In *16th Int. IEEE Conf. on Intelligent Transp. Sys.*, 2013.
[8] Dongyao Chen, Kyong-Tak Cho, Sihui Han, Zhizhuo Jin, and Kang G Shin. Invisible sensing of vehicle steering with smartphones. In *Proceedings of the 13th Annual Int. Conf. on Mobile Syst., Appl., and Services*, pages 1–13. ACM, 2015.
[9] Anup Doshi and Mohan Manubhai Trivedi. On the roles of eye gaze and head dynamics in predicting driver's intent to change lanes. 10(3):453–462, 2009.
[10] Eric M Foxlin. Head tracking relative to a moving vehicle or simulator platform using differential inertial sensors. In *AeroSense 2000*, pages 133–144. Int. Society for Optics and Photonics, 2000.
[11] Shoya Ishimaru, Kai Kunze, Koichi Kise, Jens Weppner, Andreas Dengel, Paul Lukowicz, and Andreas Bulling. In the blink of an eye: combining head motion and eye blink frequency for activity recognition with google glass. In *Proceedings of the 5th augmented human Int. Conf.*, page 15. ACM, 2014.
[12] Cagdas Karatas, Hongyu Li, and Luyang Liu. Toward detection of unsafe driving with inertial head-mounted sensors. In *Proceedings of the Eighth Wireless of the Students, by the Students, and for the Students Workshop*, pages 45–47. ACM, 2016.
[13] Cagdas Karatas, Luyang Liu, Hongyu Li, Jian Liu, Yan Wang, Sheng Tan, Jie Yang, Yingying Chen, Marco Gruteser, and Richard Martin. Leveraging wearables for steering and driver tracking. In *Comput. Commun., IEEE INFOCOM 2016-The 35th Annual IEEE Int. Conf. on*, pages 1–9. IEEE, 2016.
[14] Firas Lethaus and Jürgen Rataj. Do eye movements reflect driving manoeuvres? 1(3):199, 2007.
[15] Sugang Li, Ashwin Ashok, Yanyong Zhang, Chenren Xu, Janne Lindqvist, and Macro Gruteser. Whose move is it anyway? authenticating smart wearable devices using unique head movement patterns. In *Pervasive Computing and Commun. (PerCom), 2016 IEEE Int. Conf. on*, pages 1–9. IEEE, 2016.
[16] Luyang Liu, Cagdas Karatas, Hongyu Li, Sheng Tan, Marco Gruteser, Jie Yang, Yingying Chen, and Richard P Martin. Toward detection of unsafe driving with wearables. In *Proc. 2015 workshop on Wearable Syst. and Applicat.*, pages 27–32, 2015.
[17] Luyang Liu, Hongyu Li, Jian Liu, Cagdas Karatas, Yan Wang, Marco Gruteser, Yingying Chen, and Richard P Martin. Bigroad: Scaling road data acquisition for dependable self-driving. In *Proceedings of the 15th Annual Int. Conf. on Mobile Syst., Appl., and Services*, pages 371–384. ACM, 2017.
[18] Erik Murphy-Chutorian, Anup Doshi, and Mohan Manubhai Trivedi. Head pose estimation for driver assistance syst.: A robust algorithm and experimental evaluation. In *Intelligent Transportation Syst. Conf., 2007. ITSC 2007. IEEE*, pages 709–714. IEEE, 2007.
[19] Nuria Oliver and Alex P Pentland. Graphical models for driver behavior recognition in a smartcar. In *Intelligent Vehicles Symp., 2000. IV 2000. Proceedings of the IEEE*, pages 7–12. IEEE, 2000.
[20] Hao Pan, Yi-Chao Chen, Guangtao Xue, and Xiaoyu Ji. Magnecomm: Magnetometer-based near-field communication. In *Proceedings of the 23rd Annual International Conference on Mobile Computing and Networking*, pages 167–179. ACM, 2017.
[21] Bethany R Raiff, Çağdaş Karataş, Erin A McClure, Dario Pompili, and Theodore A Walls. Laboratory validation of inertial body sensors to detect cigarette smoking arm movements. 3(1):87–110, 2014.
[22] Nirupam Roy, He Wang, and Romit Roy Choudhury. I am a smartphone and i can tell my user's walking direction. In *Proceedings of the 12th annual international conference on Mobile systems, applications, and services*, pages 329–342. ACM, 2014.
[23] Sheng Shen, He Wang, and Romit Roy Choudhury. I am a smartwatch and i can track my user's arm. In *Proceedings of the 14th annual Int. Conf. on Mobile Syst., Appl., and services*, pages 85–96. ACM, 2016.
[24] Manbir Sodhi, Bryan Reimer, JL Cohen, E Vastenburg, R Kaars, and S Kirschenbaum. On-road driver eye movement tracking using head-mounted devices. In *Proceedings of the 2002 Symp. on Eye tracking research & Appl.*, pages 61–68. ACM, 2002.
[25] Chen Wang, Xiaonan Guo, Yan Wang, Yingying Chen, and Bo Liu. Friend or foe?: Your wearable devices reveal your personal pin. In *Proceedings of the 11th ACM on Asia Conf. on Comput. and Commun. Security*, pages 189–200. ACM, 2016.
[26] He Wang, Ted Tsung-Te Lai, and Romit Roy Choudhury. Mole: Motion leaks through smartwatch sensors. In *Proceedings of the 21st Annual Int. Conf. on Mobile Computing and Networking*, pages 155–166. ACM, 2015.
[27] Yan Wang, Yingying Jennifer Chen, Jie Yang, Marco Gruteser, Richard P Martin, Hongbo Liu, Luyang Liu, and Cagdas Karatas. Determining driver phone use by exploiting smartphone integrated sensors. *IEEE Transactions on Mobile Computing*, 15(8):1965–1981, 2016.
[28] Yan Wang, Jie Yang, Hongbo Liu, Yingying Chen, Marco Gruteser, and Richard P Martin. Sensing vehicle dynamics for determining driver phone use. In *Proceeding of the 11th annual international conference on Mobile systems, applications, and services*, pages 41–54. ACM, 2013.
[29] Jing Xiao, Tsuyoshi Moriyama, Takeo Kanade, and Jeffrey F Cohn. Robust full-motion recovery of head by dynamic templates and re-registration techniques. 13(1):85–94, 2003.
[30] Shuicheng Yan, Zhenqiu Zhang, Yun Fu, Yuxiao Hu, Jilin Tu, and Thomas Huang. Learning a person-independent representation for precise 3d pose estimation. pages 297–306, 2008.
[31] Jie Yang, Simon Sidhom, Gayathri Chandrasekaran, Tam Vu, Hongbo Liu, Nicolae Cecan, Yingying Chen, Marco Gruteser, and Richard P Martin. Sensing driver phone use with acoustic ranging through car speakers. 11(9):1426–1440, 2012.
[32] Shanhe Yi, Zhengrui Qin, and E Novak. Glassgesture: Exploring head gesture interface of smart glasses.